



Analytical modeling and dimensionless characteristics of open wet clutches in consideration of gravity

Robin Leister¹ · Amir F. Najafi² · Jochen Kriegseis¹ · Bettina Frohnappel¹ · Davide Gatti¹

Received: 18 June 2021 / Accepted: 14 September 2021 / Published online: 23 November 2021
© The Author(s) 2021

Abstract

Wet clutches are widely used in power transmission, but lack of the fact of an energy loss in open state condition. The flow conditions in the fluid flow of an open wet clutches are analyzed by analytical means. The requisite simplifications that result in an analytically integrateable solution are stated in detail. Special emphasis is put on the role of gravitation in the equations of fluid motion. This force component leads to a slightly earlier aeration than stated in earlier conditions. The simplifications and the resultant solutions are considered by means of dimensionless quantities. Despite the actual geometric parameters the drag torque can be described as $\zeta_m = \pi/Re_1$. An additional aeration condition is introduced, which is based on the back flow of the radial velocity. This quantity can be described as non-dimensional volumetric flow rate Q^* . With these equations at hand the theoretical considerations are transferred to an evaluation with grooves, where a backward curved groove appears as beneficial for further investigations.

Analytische Modellierung und dimensionslose Charakteristiken von offenen nasslaufenden Lamellenkupplungen unter Berücksichtigung der Schwerkraft

Zusammenfassung

Nasslaufende Lamellenkupplungen sind weitverbreitet in der Kraftübertragung, haben jedoch den Nachteil eines Energieverlustes im offenen Zustand. Die Strömungsverhältnisse in einer offenen nasslaufenden Lamellenkupplung werden mittels analytischer Methoden untersucht. Die notwendigen Vereinfachungen, die zu einer analytisch integrierbaren Lösung führen, werden im Detail angegeben. Besonderes Augenmerk wird auf die Rolle der Gravitation in den Gleichungen der Flüssigkeitsbewegung gelegt. Diese Kraftkomponente führt zu einem leicht früheren Lufteinzug als in früheren Bedingungen angegeben. Die Vereinfachungen und die sich daraus ergebenden Lösungen werden mit Hilfe von dimensionslosen Größen betrachtet. Unabhängig der tatsächlichen geometrischen Parameter kann das Schleppmoment beschrieben werden als $\zeta_m = \pi/Re_1$. Eine weiterführende Bedingung für den Lufteinzug wird eingeführt, welche auf der Rückströmung der Radialgeschwindigkeit beruht. Diese Größe kann als dimensionsloser Volumenstrom Q^* angegeben werden. Mit den vorliegenden Gleichungen werden die theoretischen Überlegungen auf eine Betrachtung mit Nuten übertragen, auf deren Grundlage eine rückwärtsgekrümmte Nut als vorteilhaft für weitere Untersuchungen erscheint.

1 Introduction

One major trend in recent years is the reduction of energy consumption in the automotive industry due to strict regulations and the constant demand for higher ranges of battery-powered vehicles. One field that still offers a significant potential are wet clutches, which are an integral part of nearly every higher-class automobile. In open clutch state this structural element produces a remaining torque despite its disengaged mode, due to the sub-millimeter spacing of the disks and the presence of cooling oil. This so-called

✉ Robin Leister
robin.leister@kit.edu

¹ Institute of Fluid Mechanics (ISTM), Karlsruhe Institute of Technology (KIT), Kaiserstr. 10, 76131 Karlsruhe, Germany

² School of Mechanical Engineering, College of Engineering, University of Tehran, P.O. Box 11365/4563 Tehran, Iran

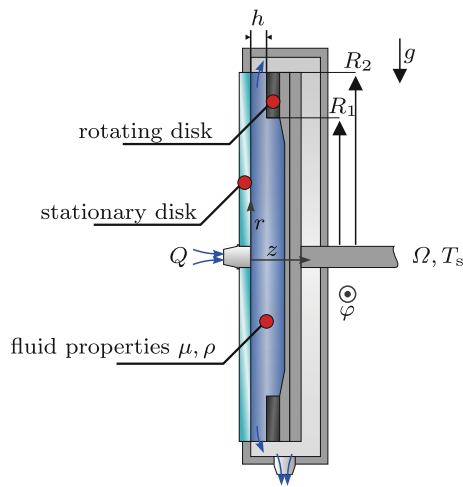


Fig. 1 Sketch of an open clutch with all geometrical and operational parameters and fluid properties

drag torque T_s is a source of energy loss, which motivated various efforts in recent years to predict and consequently minimize this adverse effect.

The potential of drag-torque reduction was first discovered in R&D departments of industrial companies, but was soon adopted from universities and research associations with applied scientific issues [10, 13]. The introduction of surface grooves on one disk shifts the operation point at which air is sucked into the gap between the disks to lower velocities. This so-called aeration is a physical key feature for the minimization of energy losses. A profound understanding of the occurrence of aeration for various groove-shaped disks is thus one essential building block for the fundamental scientific analysis of this industry-relevant flow scenario.

From an academic point of view the flow occurring in an open wet clutch can be classified as sub-millimeter gap flow scenario with a rotor-stator configuration [6, 7].

Fig. 1 provides detailed information about the geometrical configuration. For simplicity a two-disk model is considered, in which one disk is at rest, while the other is

spinning at an angular velocity Ω . Relevant geometrical quantities are the inner and the outer disk radius R_1 and R_2 , respectively and the gap height h . From a central region the cooling oil volumetric flow rate Q is fed into the system. In order to reach the state, where ambient air is sucked into the system between the two disks, the feeding capacity of the rotating disk must exceed the flow rate Q . Table 1 summarizes all relevant parameters including the corresponding physical units and specified values, which are used throughout the present work.

In general, the flow system can be addressed with analytical, numerical or experimental efforts, while all three have their advantages and drawbacks. The experimental description of the problem is almost exclusively done with torque measurements, such as [5, 13, 16, 21]. The downside of this technique is that no velocity information are incorporated in the process. The experimental approach typically relies on the acquisition of one integral value only, which renders the elaboration of a detailed cause-effect relation as well as a geometrical scaling difficult. Lately an extraction of volumetric (3D) three-component (3C) velocity information out of a two-disk open clutch model was done by the use of defocusing particle tracking velocimetry (DPTV) [8].

A detailed velocity field and fluid information within the gap flow as yet was mostly obtained via numerical analysis such as [17, 19]. Different groove designs were studied by NEUPERT et al. [11]. A simulation method, which features short simulation times and thus aims to be used at an early stage of development, was presented by GRÖTSCH et al. [2].

However the technique of numerical analysis inherently is in need of appropriate fluid flow models and the determination of partially unknown boundary conditions, which leads to a limitation of the overall informative value. A suitable and widespread approach to achieve an initial estimation of the drag torque and the start of aeration exploits simplified analytical models. These theoretical descriptions ground on a laminar flow assumption, which is most-likely to occur [1], and on simplifications of the Navier–Stokes equations (NSE), such as those presented by e.g. [3, 4, 14, 15, 20]. Due to different underlying assumptions, the resulting simplified governing equations for the velocity field differ slightly in each work. A recent comparison of the models together with experimental measurements is discussed by NEUPERT et al. [12]. A detailed analysis of the different terms in the NSE and their corresponding simplifications is provided by LEISTER et al. [9]. The related introduction of dimensionless quantities paves the way for a systematic comparison of different results, which holds likewise for both numerical or experimental data.

In continuation of these recent efforts [9], the present work extends the approach of a dimensionless description of the problem at hand through the considerations of gravitational effects. The governing equations are brought to

Table 1 Quantities of corresponding physical values for all relevant open clutch parameters

Parameter	Symbol	Physical value	Dimension
Inner radius	R_1	8.25×10^{-2}	[m]
Outer radius	R_2	9.375×10^{-2}	[m]
Volume flow rate	Q	1.667×10^{-5}	[m ³ s ⁻¹]
Density	ρ	850	[kg m ⁻³]
Dyn. viscosity	μ	0.0136	[Pa s]
Kin. viscosity	ν	16×10^{-6}	[m ² s ⁻¹]
Gap height	h	450×10^{-6}	[m]
Angular velocity	Ω	$0 < \Omega < 314$	[1 s ⁻¹]
Grav. acceleration	g	9.81	[m s ⁻²]

Table 2 Characteristic velocities and length scales for the order-of-magnitude analysis conducted in Eqs. (1)–(3)

Parameter	Symbol	Characteristic quantity
Radial flow rate	u_r	$u_r = \frac{q}{R}$
Circumferential velocity	u_φ	ΩR
Axial velocity	u_z	$u_z = u_r \frac{h}{R} = \frac{qh}{R^2}$
Radial direction	R	$R = \frac{R_1+R_2}{2}$
Axial direction	h	h

a dimensionless form and existing aeration conditions are discussed in this context. As a result, a single equation is developed whose solution allows to predict drag torque as well as the start of aeration for test rigs with different geometrical dimensions. This dimensionless setting thus also allows for a direct comparison of results obtained in different test rigs. Finally, in the last part of the paper, a recommended shape orientation of surface grooves is derived from streamline evaluations.

2 Analytical derivation

In cylindrical coordinates the Navier–Stokes equations or momentum conservation for a steady flow of a Newtonian fluid in radial, circumferential and axial direction (r, φ and z component) can be seen in Eqs. (1)–(3). Note that the orientation of gravity is shown in Fig. 1. The order of magnitudes are indicated above each term. The characteristic velocities and length scales are summarized in Table 2. The local disk velocity ΩR is chosen as characteristic velocity along the circumferential direction, while the imposed volume flow rate per unit depth, referred to as q , is the radial velocity scale. The characteristic axial velocity follows from dimensional analysis of the continuity equation under the assumption that the gravitational force does not cause significant loss of axial symmetry in azimuthal velocity, i.e. that the term $\frac{1}{R} \frac{\partial u_\varphi}{\partial \varphi}$ can be neglected.

(1):

$$\begin{aligned}
 & \underbrace{\mathcal{O}\left(\frac{q^2}{R^3}\right)}_{u_r \frac{\partial u_r}{\partial r}} + \underbrace{\mathcal{O}\left(\frac{\Omega q}{R}\right)}_{\frac{u_\varphi}{r} \frac{\partial u_r}{\partial \varphi}} - \underbrace{\mathcal{O}(\Omega^2 R)}_{\frac{u_\varphi^2}{r}} + \underbrace{\mathcal{O}\left(\frac{q^2}{R^3}\right)}_{u_z \frac{\partial u_r}{\partial z}} \\
 &= -\frac{1}{\rho} \frac{\partial p}{\partial r} + v \frac{\partial}{\partial r} \left[\frac{1}{r} \frac{\partial}{\partial r} (ru_r) \right] + \frac{\mathcal{O}\left(\frac{vq}{R^3}\right)}{r^2} \frac{\partial^2 u_r}{\partial \varphi^2} \\
 & \quad - \frac{\mathcal{O}\left(\frac{v\Omega}{R}\right)}{r^2} \frac{\partial u_\varphi}{\partial \varphi} + v \frac{\mathcal{O}\left(\frac{vq}{Rh^2}\right)}{\partial z^2} + g_r,
 \end{aligned} \tag{1}$$

(2):

$$\begin{aligned}
 & \underbrace{\mathcal{O}\left(\frac{q\Omega}{R}\right)}_{u_r \frac{\partial u_\varphi}{\partial r}} + \underbrace{\mathcal{O}(\Omega^2 R)}_{\frac{u_\varphi}{r} \frac{\partial u_\varphi}{\partial \varphi}} + \underbrace{\mathcal{O}\left(\frac{q\Omega}{R}\right)}_{\frac{u_r u_\varphi}{r}} + \underbrace{\mathcal{O}\left(\frac{q\Omega}{R}\right)}_{u_z \frac{\partial u_\varphi}{\partial z}} \\
 &= -\frac{1}{\rho r} \frac{\partial p}{\partial \varphi} + v \frac{\partial}{\partial r} \left[\frac{1}{r} \frac{\partial}{\partial r} (ru_\varphi) \right] + \frac{\mathcal{O}\left(\frac{v\Omega}{R}\right)}{r^2} \frac{\partial^2 u_\varphi}{\partial \varphi^2} \\
 & \quad + \frac{\mathcal{O}\left(\frac{vq}{R^3}\right)}{r^2} \frac{\partial u_r}{\partial r} + v \frac{\mathcal{O}\left(\frac{v\Omega R}{h^2}\right)}{\partial z^2} + g_\varphi,
 \end{aligned} \tag{2}$$

(3):

$$\begin{aligned}
 & \underbrace{\mathcal{O}\left(\frac{q^2 h}{R^4}\right)}_{u_r \frac{\partial u_z}{\partial r}} + \underbrace{\mathcal{O}\left(\frac{\Omega q h}{R^2}\right)}_{\frac{u_\varphi}{r} \frac{\partial u_z}{\partial \varphi}} + \underbrace{\mathcal{O}\left(\frac{q^2 h}{R^4}\right)}_{u_z \frac{\partial u_z}{\partial z}} \\
 &= -\frac{1}{\rho} \frac{\partial p}{\partial z} + v \left[\frac{1}{r} \frac{\partial}{\partial r} \left(r \frac{\partial u_z}{\partial r} \right) \right] + \frac{\mathcal{O}\left(\frac{vqh}{R^4}\right)}{r^2} \frac{\partial^2 u_z}{\partial \varphi^2} + v \frac{\mathcal{O}\left(\frac{vq}{R^2 h}\right)}{\partial z^2}.
 \end{aligned} \tag{3}$$

In order to obtain the relevant dimensionless numbers, the order of magnitudes of Eqs. (1) and (2) are normalized by the order of magnitude of their fifth term of the right hand side of the respective equation and Eq. (3) is divided by the order of magnitude of the fourth term of the equation. The resulting dimensionless numbers are given as order-of-magnitude factors in Eqs. (4)–(6). Here, $\alpha = \frac{q}{\Omega R^2}$, $Re_g = \frac{h^2 \Omega}{\nu}$ and $Fr = \frac{\Omega^2 R}{g}$ were introduced for further simplification. α is the ratio of the characteristic radial and circumferential velocity, while Re_g and Fr are the gap Reynolds number and the Froude number based on the radius as characteristic length, respectively.

(4):

$$\begin{aligned}
 & \underbrace{\mathcal{O}(\alpha Re_g)}_{\frac{\partial u_r}{\partial r}} + \underbrace{\mathcal{O}(Re_g)}_{\frac{u_\varphi}{r} \frac{\partial u_r}{\partial \varphi}} - \underbrace{\mathcal{O}\left(\frac{Re_g}{\alpha}\right)}_{\frac{u_\varphi^2}{r}} + \underbrace{\mathcal{O}(\alpha Re_g)}_{u_z \frac{\partial u_r}{\partial z}} \\
 &= -\frac{1}{\rho} \frac{\partial p}{\partial r} + v \frac{\partial}{\partial r} \left[\frac{1}{r} \frac{\partial}{\partial r} (ru_r) \right] + \frac{\mathcal{O}\left(\frac{h^2}{R^2}\right)}{r^2} \frac{\partial^2 u_r}{\partial \varphi^2} \\
 & \quad - \frac{\mathcal{O}\left(\frac{h^2}{\alpha R^2}\right)}{r^2} \frac{\partial u_\varphi}{\partial \varphi} + v \frac{\mathcal{O}(1)}{\partial z^2} + \frac{\mathcal{O}\left(\frac{Re_g}{Fr \alpha}\right)}{g_r},
 \end{aligned} \tag{4}$$

(φ):

$$\begin{aligned} & \underbrace{u_r \frac{\partial u_\varphi}{\partial r}}_{\mathcal{O}(\alpha \text{Re}_g)} + \underbrace{\frac{u_\varphi}{r} \frac{\partial u_\varphi}{\partial \varphi}}_{\mathcal{O}(\text{Re}_g)} + \underbrace{\frac{u_r u_\varphi}{r}}_{\mathcal{O}(\alpha \text{Re}_g)} + \underbrace{u_z \frac{\partial u_\varphi}{\partial z}}_{\mathcal{O}(\alpha \text{Re}_g)} \\ &= -\frac{1}{\rho r} \frac{\partial p}{\partial \varphi} + \underbrace{v \frac{\partial}{\partial r} \left[\frac{1}{r} \frac{\partial}{\partial r} (r u_\varphi) \right]}_{\mathcal{O}\left(\frac{h^2}{R^2}\right)} + \underbrace{\frac{v}{r^2} \frac{\partial^2 u_\varphi}{\partial \varphi^2}}_{\mathcal{O}\left(\frac{h^2}{R^2}\right)} \\ &+ \underbrace{\frac{2v}{r^2} \frac{\partial u_r}{\partial \varphi}}_{\mathcal{O}\left(\frac{\alpha h^2}{R^2}\right)} + \underbrace{v \frac{\partial^2 u_\varphi}{\partial z^2}}_{\mathcal{O}(1)} + \underbrace{g \cos \varphi}_{\mathcal{O}\left(\frac{\text{Re}_g}{\text{Fr}}\right)}, \end{aligned} \quad (5)$$

(z):

$$\begin{aligned} & \underbrace{u_r \frac{\partial u_z}{\partial r}}_{\mathcal{O}(\alpha \text{Re}_g)} + \underbrace{\frac{u_\varphi}{r} \frac{\partial u_z}{\partial \varphi}}_{\mathcal{O}(\text{Re}_g)} + \underbrace{u_z \frac{\partial u_z}{\partial z}}_{\mathcal{O}(\alpha \text{Re}_g)} \\ &= -\frac{1}{\rho} \frac{\partial p}{\partial z} + \underbrace{v \left[\frac{1}{r} \frac{\partial}{\partial r} \left(r \frac{\partial u_z}{\partial r} \right) \right]}_{\mathcal{O}\left(\frac{h^2}{R^2}\right)} + \underbrace{\frac{v}{r^2} \frac{\partial^2 u_z}{\partial \varphi^2}}_{\mathcal{O}\left(\frac{h^2}{R^2}\right)} + \underbrace{v \frac{\partial^2 u_z}{\partial z^2}}_{\mathcal{O}(1)}. \end{aligned} \quad (6)$$

Based on the relevant dimensionless numbers in the governing equations, simplifications can now be performed. The following assumptions can be applied to this flow:

- (i) $h/R \ll 1$,
- (ii) $\text{Re}_g \ll 1$,
- (iii) $\text{Re}_g \gg \alpha$,

The first assumption is valid for nearly all gap flow scenarios, especially when considering sub-millimeter gaps. The second assumption can also be considered to be of general validity for the application at hand, since the typical region for an angular velocity ranges at $0 < n < 3000$. The third assumption depends on the magnitude of Ω and can be considered to hold true in the present case since aeration typically occurs at high circumferential speed. The role of the Froude-number Fr deserves a separate consideration. With the three assumptions described above, the three partial differential equations Eqs. (4)–(6) reduce to

$$\underbrace{-\frac{u_\varphi^2}{r}}_{\mathcal{O}\left(\frac{\text{Re}_g}{\alpha}\right)} = -\frac{1}{\rho} \frac{\partial p}{\partial r} + \underbrace{v \frac{\partial^2 u_r}{\partial z^2}}_{\mathcal{O}(1)} - \underbrace{g \cos \varphi}_{\mathcal{O}\left(\frac{\text{Re}_g}{\text{Fr} \alpha}\right)} \quad (7)$$

$$0 = -\frac{1}{r \rho} \frac{\partial p}{\partial \varphi} + \underbrace{v \frac{\partial^2 u_\varphi}{\partial z^2}}_{\mathcal{O}(1)} + \underbrace{g \sin \varphi}_{\mathcal{O}\left(\frac{\text{Re}_g}{\text{Fr}}\right)} \quad (8)$$

$$0 = -\frac{1}{\rho} \frac{\partial p}{\partial z} + \underbrace{v \frac{\partial^2 u_z}{\partial z^2}}_{\mathcal{O}(1)}. \quad (9)$$

In order to solve this system of partial differential equations with analytical methods, further assumptions need to be taken. All partial derivatives of the pressure could in theory depend on the other spatial coordinates, which renders an integration impossible. A common way to overcome this issue is the consideration of vorticity transport, which again includes three equations, one for each spatial direction. Considering the already introduced simplifications these equations in r and φ -direction can be written as:

$$0 = \underbrace{\frac{v}{r} \frac{\partial^3 u_z}{\partial z^2 \partial \varphi}}_{\mathcal{O}\left(\frac{\alpha h^2}{R^2}\right)} - \underbrace{v \frac{\partial^3 u_\varphi}{\partial z^3}}_{\mathcal{O}(1)}, \quad (10)$$

$$\underbrace{-\frac{1}{r} \frac{\partial u_\varphi^2}{\partial z}}_{\mathcal{O}\left(\frac{\text{Re}_g}{\alpha}\right)} = \underbrace{v \frac{\partial^3 u_r}{\partial z^3}}_{\mathcal{O}(1)} + \underbrace{v \frac{\partial^2 u_z}{\partial z^2 \partial r}}_{\mathcal{O}\left(\frac{h^2}{R^2}\right)}. \quad (11)$$

An order-of-magnitude analysis with the above-listed assumptions (i–iii) and a partial integration along z of both equations yields an additional integration term, which is no function of z .

$$0 = -v \frac{\partial^2 u_\varphi}{\partial z^2} + f_r(r, \varphi) \quad (12)$$

$$\frac{u_\varphi^2}{r} = v \frac{\partial^2 u_r}{\partial z^2} + f_\varphi(r, \varphi) \quad (13)$$

A simple term-wise comparison with Eqs. (7)–(8) yields the conclusion that the pressure gradient in r -direction is not a function of z . The same holds for the pressure gradient in φ -direction. So Eqs. (7) and (8) can be integrated over z assuming a constant pressure gradient along z .

Following the initial assumption that $\frac{1}{R} \frac{\partial u_\varphi}{\partial \varphi}$ in the continuity equation can be neglected, the pressure gradient in φ -direction exactly balances with the gravitational force in that direction. In other words, the first term and third term on the right hand side of Eq. (8) are equal and thus cancel in the equation. Overall, the order-of-magnitude analysis along with the introduced assumptions results in a differential system, which can be written as:

$$-\frac{u_\varphi^2}{r} = -\frac{1}{\rho} \frac{\partial p}{\partial r} + v \frac{\partial^2 u_r}{\partial z^2} - g \cos \varphi \quad (14)$$

$$0 = v \frac{\partial^2 u_\varphi}{\partial z^2} \quad (15)$$

$$0 = -\frac{1}{\rho} \frac{\partial p}{\partial z} + v \frac{\partial^2 u_z}{\partial z^2}. \quad (16)$$

These equations are similar to the earlier findings [9], but the gravitational force in the r -component now appears as additional term.

Since the pressure gradient $\frac{\partial p}{\partial r}$ is not a function of z , the equations can be integrated and solved analytically, which yields:

$$u_\varphi(r, z) = \Omega r \frac{z}{h} \tag{17}$$

$$u_r(r, \varphi, z) = \frac{\Omega^2 r h}{12\nu} \left(z - \frac{z^4}{h^3} \right) - \frac{h}{2\mu} \frac{\partial p}{\partial r} \left(z - \frac{z^2}{h} \right) - \frac{gh}{2\nu} \cos \varphi \left(z - \frac{z^2}{h} \right). \tag{18}$$

The pressure gradient can be determined due to the fact that the supplied volumetric flow rate Q is a known quantity. An integral of the radial velocity along the axial and circumferential component leads to

$$Q = \text{const.} = \int_0^{2\pi} \int_0^h u_r r \, dz d\varphi = -\frac{\pi h^3}{6\mu} \frac{\partial p}{\partial r} + \frac{\pi r^2 h^3 \Omega^2}{20\nu}. \tag{19}$$

Thus the pressure component can be determined to

$$\Leftrightarrow \frac{\partial p}{\partial r} = -\frac{6\mu Q}{\pi h^3 r} + \frac{3\rho\Omega^2 r}{10}. \tag{20}$$

3 Dimensionless analysis with gravitation

3.1 Formulation of dimensionless quantities

As shown in Fig. 1 eight parameters influence the flow in an open wet clutch. A dimensional analysis (further explanation e.g. [18]) reduces these interdependencies to six dimensionless quantities, which are namely given as:

$$G = \frac{h}{R_2} \quad \text{gap ratio,} \tag{21a}$$

$$\beta = \frac{R_1}{R_2} \quad \text{radii ratio,} \tag{21b}$$

$$\text{Re}_1 = \frac{R_2 h \Omega}{\nu} \quad \text{lubrication Reynolds number,} \tag{21c}$$

$$Q^* = \frac{Q\nu}{\Omega^2 R_2^2 h^3} \quad \text{dimensionless flow rate,} \tag{21d}$$

$$\zeta_m = \frac{T_s}{\frac{\rho}{2} R_2^5 \Omega^2 (1 - \beta^4)} \quad \text{moment coefficient,} \tag{21e}$$

$$\text{Fr} = \frac{\Omega^2 R_2}{g} \quad \text{Froude number.} \tag{21f}$$

Small values of G identify flows in the gap flow category. For an open wet clutch, this value is typically in the order of 10^{-3} – 10^{-2} . The radii ratio β serves as auxiliary parameter for the drag torque calculation, since the most significant

amount of torque is generated between these two radii. The lubrication Reynolds number Re_1 is ideally suited to describe the dimensionless torque as discussed in Sect. 3.1.1. The dimensionless flow rate Q^* will serve as key parameter for the aeration condition in Sect. 3.1.2. Finally, the moment coefficient ζ_m characterizes the drag torque as a function of Ω , or Re_1 in a dimensionless consideration. Here the geometrical parameter β is already added, which reduces the calculation effort later on. With the help of these dimensionless numbers the formulation of the drag torque and aeration condition can be rewritten in a form which does not depend on the physical size and speed of a particular test rig.

3.1.1 Drag torque

The drag torque T_s as key factor for open clutch flow discussion is calculated by

$$T_s = \iint_A \mu \frac{\partial u_\varphi}{\partial z} r \, dA = 2\pi\mu \int_{R_1}^{R_2} \left(\frac{\Omega r}{h} \right) r^2 \, dr = \frac{\pi\mu\Omega}{2h} (R_2^4 - R_1^4) \tag{22}$$

With the use of this equation the moment coefficient Eq. (21e) can be rewritten to

$$\zeta_m = \frac{\pi}{\text{Re}_1}. \tag{23}$$

Thus, the dimensionless reformulation provides a simple formulation to directly estimate the drag torque. This formulation is particularly valuable for the comparison of setups with different geometrical dimensions. Instead of using a $T_s - \Omega$ diagram, which is normally done, a dimensionless $\zeta_m - \text{Re}_1$ diagram allows a direct comparison of data gained with different geometrical or fluid parameters.

3.1.2 Aeration condition

An aeration condition that is frequently used to mathematically describe the start of aeration is the sign change of the pressure gradient (e.g.[3, 4]). This state occurs normally at the outer radius first, since the pressure is lower at this point. This condition results in a formulation of the critical angular velocity $\Omega_{c,1}$ for the aeration start.

$$\frac{\partial p}{\partial r} (r = R_2, \Omega = \Omega_{c,1}) \stackrel{!}{=} 0 = -\frac{6\mu Q}{\pi h^3 r} + \frac{3\rho\Omega_{c,1}^2 r}{10} \tag{24}$$

This expression, in which dimensional geometrical and flow parameters appear explicitly, can be further shortened and simplified to one simple equation through the introduction of dimensionless numbers.

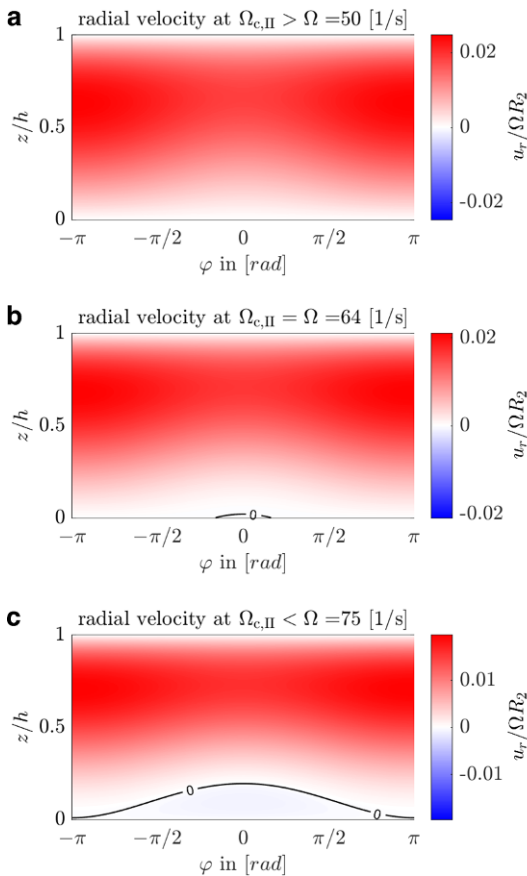


Fig. 2 Radial velocity u_r for three different distinct angular velocities Ω for **a**, at **b**, after **c** a backwards flow occurs. The occurrence of the start of a backwards flow can be located at the stationary disk at $\varphi = 0$, which is the upper side of the open clutch model

The dimensionless formulation is given by

$$Q^* = \frac{Qv}{\Omega_{c,I}^2 R_2^2 h^3} = \frac{\pi}{20}. \tag{25}$$

Since now the gravitational force is part of the calculations an additional downside of this aeration condition takes effect. This model can't resolve the role of gravity to a different start of aeration, since the pressure gradient in r -direction is axis symmetric in φ -direction.

An aeration formulation that is more likely from a fluid mechanics perspective is the occurrence of back flow of the radial velocity, which is in a normal pipe flow equal to the sign change of the pressure gradient, but due to additional force components not in this flow case. This condition will be introduced as second aeration model. Given the applied

boundary conditions the reverse flow will occur at $z = 0$. The mathematical formulation yields

$$\begin{aligned} \frac{\partial u_r}{\partial z} (z = 0, r = R_2, \Omega = \Omega_{c,II}) &\stackrel{!}{=} 0 \\ &= \frac{\Omega_{c,II}^2 R_2 h}{12\nu} - \frac{h}{2\mu} \frac{\partial p}{\partial r} - \frac{gh}{2\nu} \cos \varphi \end{aligned} \tag{26}$$

with the formulation of the pressure gradient (Eq. 20) and the reformulation with the help of the dimensionless flow rate Q^* and the Froude number Fr this equals

$$\begin{aligned} 0 &= \frac{\Omega_{c,II}^2 R_2 h}{12\nu} - \frac{3Q}{\pi h^2 R_2} - \frac{3\rho\Omega_{c,II}^2 R_2 h}{20\mu} - \frac{gh}{2\nu} \cos \varphi \\ \Leftrightarrow \frac{1}{45} &= \frac{Qv}{h^3 R_2^2 \Omega_{c,II}^2 \pi} - \frac{g \cos \varphi}{6\Omega_{c,II}^2 R_2} \\ \Leftrightarrow \frac{\pi}{45} &= Q^* - \frac{\pi}{6} \cos \varphi \frac{1}{Fr}. \end{aligned} \tag{27}$$

This aeration model in fact supports gravitational effects as well as a localization of the aeration start. If a test rig is placed as indicated in Fig. 1 the aeration starts at the highest point of the disk. This might be beneficial information for experimental investigation, since a detailed localization can be investigated easier in terms of optical access and image resolution. Fig. 2 shows the radial velocity across the gap for three different angular velocities Ω with an indicated line for the velocity $u_r = 0$, which serves as criterion for a back flow.

The dimensionless formulation is a useful way of describing the outcomes of the analytical modeling. A imminent advantage is the possibility to transfer experimental and numerical findings to a dimensionless frame of reference, to directly compare and evaluate the quality of the made simplifications or the accordance of the results.

4 Consideration of grooves

The fact that the introduction of grooves on one of the disks lead to an earlier start of aeration at lower circumferential speed has been discussed extensively in literature, lately summarized by NEUPERT et al. [11, 12], for instance. The shape of the grooves and their specific design did not reach a fundamental understanding from the fluid mechanics point of view and is currently often a choice of experience for a clutch manufacturer.

In general, the addition of a groove pattern locally increases the cross section through which the fluid can pass on its way from the inner to the outer radius. The interplay of different force components, like inertia, centrifugal and frictional force is shifted to another equilibrium due to the presence of grooves. The analytical solutions might not be the perfect tool to accurately describe the variety

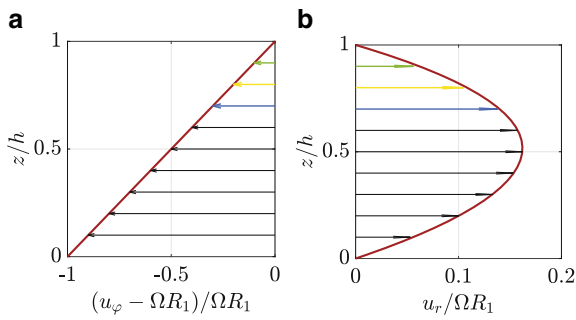


Fig. 3 **a** normalized circumferential velocity in a disk-fixed frame of reference **b** normalized radial velocity; The velocity values at 0.7–0.9*h* are color coded to fit to Fig. 4

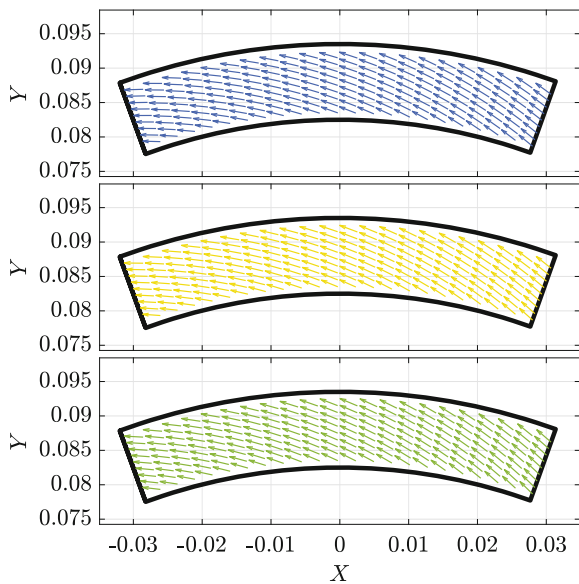


Fig. 4 Normalized relative velocity $u_\varphi - \Omega r$ and u_r for different heights above the rotating disk. (• 0.7 z/h , • 0.8 z/h and • 0.9 z/h) The colors correspond to the z/h -levels in Fig. 3

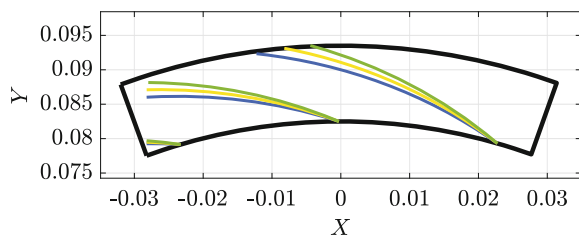


Fig. 5 Streamlines originating at $r = R_1$ and the corresponding normalized height • 0.7 z/h , • 0.8 z/h and • 0.9 z/h

of different groove patterns. To systematically differentiate various groove patterns, experimental and numerical investigations must be carried out. An analytical model cannot describe complex flow phenomena, like e.g. the vortical system found in the cavity of a radial groove [8].

However, the model can lead to basic findings that clarify the effect of grooves for an initial understanding. This

holistic view on the groove geometry is discussed under certain aspects in the following, to achieve an insight that seems appropriate to the level of detail of analytical solutions. For the following analysis, it is assumed that the overall flow pattern can be described with the analytical solution derived for a smooth disk even when grooves are applied to the rotating disk.

Fig. 3 shows the radial and relative circumferential velocity, u_r and u_φ extracted from the analytical solution, where the gravitational term is neglected. Note that for the circumferential velocity a change of the reference frame to a disk-fixed coordinate system took place. Thus in the figure, the rotating disk features a relative velocity of 0.

Fig. 4 shows the velocity at different heights in the vicinity of the moving disk ($\Omega = 10$), where a potential groove would be placed. For visual aspects a $x - y$ coordinate system is used and only a region of $\varphi \in [-10^\circ; 10^\circ]$ is plotted. Despite the fact that the velocities are localized at • 0.7 z/h , • 0.8 z/h and • 0.9 z/h , all share a similar direction. Thus, when considering a fluid particle, which starts from the inner radius and moves to the outer radius, the actual height does not affect the shape of the streamlines/path lines significantly. This fact is supported by Fig. 5, where the streamlines of the above-stated heights are shown. The streamlines start at $r = R_1$ and the corresponding height. A given angular velocity consequently produces similar streamlines for the near-wall region. Under the assumption that the flow with and without grooves are similar, a potential successful groove shape can be modeled to follow the shape of the streamlines in the disk-near region. An ideally minimum deviation from this path could be reached if the groove shape, that is also moving with the rotating disk, has the same shape than the streamlines/path lines. This shape has the benefit that the introduction of a groove does not disturb the streamlines, which leads to an outflow without losses and, thus, to an earlier aeration.

However, the exact shape is only valid for the considered parameter combination and operating point ($\Omega = 10$). This in fact could be used as benefit, since an accurate fine-adjustment is possible for a desired operating point. For further investigations, into a detailed aeration prediction the analytical concept, with its strong simplifications is not the right concept. Here experimental or numerical tools must take over, especially when the groove height and width changes along the radius to reach a minimum deviation from the streamlines of a disk without grooves. For future groove design a check of the expected aeration point and the corresponding streamline curvatures might be of interest to reach a drag reduction at the desired operation condition, which is valuable knowledge in early-stage designing process for a clutch disk manufacturer. With this information also already existing groove designs, like waffle, sunburst or group-parallel, can be cross-checked of their

suitability in each specific scenario of application with its individual needs. The general groove design of a backward curved groove, however, serves as starting point for a future in-depth analysis.

5 Conclusion

The simplifications required to reach an analytically integrable partial differential system for open wet clutch flows in consideration of gravitational forces have been outlined in detail. Two dimensionless key factors are the gap Reynolds number Re_g and the ratio of radial flow compared to circumferential flow α . Both quantities need to be small in order to reach the concluded simplifications. The consideration of the gravitational force impacts only the radial velocity component. With this force component an aeration will occur earlier, based on the aeration condition of a reverse flow at the stationary disk. Six dimensionless numbers are identified, that enable a fast calculation of drag torque and aeration without solving complex equations. The dimensionless drag torque can be rewritten to $\zeta_m = \frac{\pi}{Re_g}$, while the aeration onset based on a reversed flow at the stationary disk can be described via $Q^* - \frac{\pi \cos \varphi}{6 Fr}$. The aeration thus starts at $\varphi = 0$ when gravitation acts on a test rig in upright position. This knowledge might be particular beneficial for future experimental investigations. The consideration of grooves on the surface of the rotating disks is done via a holistic view by means of streamlines in the vicinity of $z/h = 1$. A backward curved along the radius r is suggested, since the groove shape follows the streamlines in this case. This information, despite the simplicity of the considered approach, provides a valuable guideline for clutch pattern design beyond existing engineering tools.

Funding Open Access funding enabled and organized by Projekt DEAL.

Conflict of interest The authors declare that they have no conflict of interest.

Open Access This article is licensed under a Creative Commons Attribution 4.0 International License, which permits use, sharing, adaptation, distribution and reproduction in any medium or format, as long as you give appropriate credit to the original author(s) and the source, provide a link to the Creative Commons licence, and indicate if changes were made. The images or other third party material in this article are included in the article's Creative Commons licence, unless indicated otherwise in a credit line to the material. If material is not included in the article's Creative Commons licence and your intended use is not permitted by statutory regulation or exceeds the permitted use, you will need to obtain permission directly from the copyright holder. To view a copy of this licence, visit <http://creativecommons.org/licenses/by/4.0/>.

References

- Daily JW, Nece RE (1960) Chamber dimension effects on induced flow and frictional resistance of enclosed rotating disks. *J Basic Eng* 82(1):217–230. <https://doi.org/10.1115/1.3662532>
- Grötsch D, Niedenthal R, Völkel K, Pflaum H, Stahl K (2019) Effiziente CFD-Simulationen zur Berechnung des Schleppmoments nasslaufender Lamellenkupplungen im Abgleich mit Prüfstandmessungen. *Forsch Ingenieurwes* 83:227–237. <https://doi.org/10.1007/s10010-019-00302-3>
- Huang J, Wei J, Qiu M (2012) Laminar flow in the gap between two rotating parallel frictional plates in hydro-viscous drive. *Chin J Mech Eng* 25(1):144–152. <https://doi.org/10.3901/CJME.2012.01.144>
- Iqbal S, Al-Bender F, Pluymers B, Desmet W (2013) Model for predicting drag torque in open multi-disks wet clutches. *J Fluids Eng* 136(2):21103. <https://doi.org/10.1115/1.4025650>
- Jibin H, Zengxiang P, Chao W (2012) Experimental research on drag torque for single-plate wet clutch. *J Tribol* 134:14502. <https://doi.org/10.1115/1.4005528>
- Lance GN, Rogers MH (1962) The axially symmetric flow of a viscous fluid between two infinite rotating disk. *Proceedings of the Royal Society of London. Series A, Mathematical and Physical Sciences* 266(1324), 109–121. <http://www.jstor.org/stable/2414223>. Accessed 13 Mar 2018
- Lauder, B., Poncelet, S., Serre, E.: Laminar, transitional, and turbulent flows in rotor-stator cavities. *Annual Review of Fluid Mechanics* 42(1), 229–248 (2010). <https://doi.org/10.1146/annurev-fluid-121108-145514>. <https://doi.org/10.1146/annurev-fluid-121108-145514>
- Leister, R., Fuchs, T., Mattern, P., Kriegseis, J.: Flow-structure identification in a radially grooved open wet clutch by means of defocusing particle tracking velocimetry. *Experiments in fluids* 62(2), Article: 29 (2021). <https://doi.org/10.1007/s00348-020-03116-0>
- Leister R, Najafi AF, Gatti D, Kriegseis J, Frohnapfel B (2020) Non-dimensional characteristics of open wet clutches for advanced drag torque and aeration predictions. *Tribol Int* 152:106442. <https://doi.org/10.1016/j.triboint.2020.106442>
- Lloyd F (1974) Parameters contributing to power loss in disengaged wet clutches. In: *SAE Technical Paper Series*. SAE International. <https://doi.org/10.4271/740676>. Accessed 19 Aug 2018
- Neupert T, Bartel D (2019) High-resolution 3d cfd multiphase simulation of the flow and the drag torque of wet clutch discs considering free surfaces. *Tribol Int* 129:283–296. <https://doi.org/10.1016/j.triboint.2018.08.031>
- Neupert T, Benke E, Bartel D (2018) Parameter study on the influence of a radial groove design on the drag torque of wet clutch discs in comparison with analytical models. *Tribol Int* 119:809–821. <https://doi.org/10.1016/j.triboint.2017.12.005>
- Oerleke C, Funk W (2000) Leerlaufverhalten ölgekühlter Lamellenkupplungen – Abschlußbericht. *Berichtszeitraum* 290:1995–1998
- Pahlovy S, Mahmud S, Kubota M, Ogawa M, Takakura N (2016) Prediction of drag torque in a disengaged wet clutch of automatic transmission by analytical modeling. *Tribol Online Japanes Soc Tribol* 11(2):121–129. <https://doi.org/10.2474/trol.11.121>
- Rao G (2010) Modellierung und Simulation des Systemverhaltens nasslaufender Lamellenkupplungen. *Dissertation*, Technische Universität Dresden, Dresden
- Takagi Y, Okano Y, Miyayaga M, Katayama N (2012) Numerical and physical experiments on drag torque in a wet clutch. *Tribol Online* 7(4):242–248. <https://doi.org/10.2474/trol.7.242>
- Wu W, Xiong Z, Hu J, Yuan S (2015) Application of cfd to model oil–air flow in a grooved two-disc system. *Int J Heat Mass Transf* 91:293–301. <https://doi.org/10.1016/j.ijheatmasstransfer.2015.07.092>

18. Yarin LP (2012) The Pi-theorem : applications to fluid mechanics and heat and mass transfer. Experimental fluid mechanics. Springer, Berlin <https://doi.org/10.1007/978-3-642-19565-5>
19. Yuan Y, Attibele P, Dong Y (2003) Cfd simulation of the flows within disengaged wet clutches of an automatic transmission. In. SAE, vol 2003. SAE International, World Congress & Exhibition <https://doi.org/10.4271/2003-01-0320>
20. Yuan Y, Liu EA, Hill J, Zou Q (2006) An improved hydrodynamic model for open wet transmission clutches. J Fluids Eng 129(3):333–337. <https://doi.org/10.1115/1.2427088>
21. Zhou X, Walker P, Zhang N, Zhu B, Ruan J (2014) Numerical and experimental investigation of drag torque in a two-speed dual clutch transmission. Mech Mach Theory 79:46–63. <https://doi.org/10.1016/j.mechmachtheory.2014.04.007>